

The first two leading modes of the tropical Pacific and their linkage without global warming

Yang Li¹, QuanLiang Chen^{1*}, XiaoRan Liu², Nan Xing³, ZhiGang Cheng¹, HongKe Cai¹, Xin Zhou¹, Dong Chen¹, XiaoFei Wu¹, and MingGang Li¹

¹College of Atmospheric Science, Plateau Atmosphere and Environment Key Laboratory of Sichuan Province, Chengdu University of Information Technology, Chengdu 610225, China;

²State Chongqing Climate Center, Chongqing 401147, China;

³Beijing Meteorological Service, Beijing 100875, China

Abstract: A discrepancy remains in the first two leading empirical orthogonal function (EOF) modes of the tropical Pacific sea surface temperature anomaly (SSTA) based on observations since the 1980s. The EOF1 mode, representing the El Niño-Southern Oscillation (ENSO), is a robust result. However, the EOF2 features either El Niño Modoki (EM) or ENSO evolution during different periods, which is probably associated with the impacts of global warming. The underlying question is what the EOF2 mode of the tropical Pacific would be without global warming. Using the CMIP5 preindustrial scenario to exclude the influence of global warming, we find that the EOF1 mode of the tropical Pacific SSTA represents ENSO and that the EOF2 mode is not EM. According to the lead-lag correlation between the ENSO and EOF2 modes, the linkage between these two modes is as follows: ...El Niño → EOF2 → La Niña → -EOF2 → El Niño.... By analyzing the evolution of sea surface temperature, surface wind, and subsurface ocean temperature anomalies, we find the mechanism linking the ENSO and EOF2 modes is the air-sea interaction associated with the ENSO cycle. This result suggests that the EOF2 mode represents an aspect of ENSO evolution under preindustrial conditions. Therefore, this study further indicates that the EM is probably due to the influence of global warming.

Keywords: El Niño-Southern Oscillation (ENSO); ENSO evolution; global warming; air-sea interaction

Citation: Li, Y., Chen, Q. L., Liu, X. R., Xing, N., Cheng, Z. G., Cai, H. K., Zhou, X., Chen, D., Wu, X. F., and Li, M. G. (2019). The first two leading modes of the tropical Pacific and their linkage without global warming. *Earth Planet. Phys.*, 3(2), 157–165.

<http://doi.org/10.26464/epp2019019>

1. Introduction

The El Niño-Southern Oscillation (ENSO) is a large-scale air-sea interaction over the central and eastern tropical Pacific (Bjerknes, 1969). There is widespread public concern that this mode of climate variability should be understood because the prediction of ENSO plays an important role in the prediction of global climate anomalies (Zheng F et al., 2006; Zheng F and Zhu J, 2016; Zheng F and Yu JY, 2017). For instance, ENSO conditions influence the Asian-Australian summer monsoon (e.g., Li JP et al., 2012; Yang RW et al., 2017, 2019) and Pacific-North American teleconnections (e.g., Wallace and Gutzler, 1981). Recently, a new El Niño phenomenon, referred to as El Niño Modoki (EM), dateline El Niño, Central Pacific El Niño, or warm pool El Niño, has been found to occur frequently in the tropical Pacific (Larkin and Harrison, 2005; Ashok et al., 2007; Kao HY and Yu JY, 2009; Kug et al., 2009; Yeh et al., 2009; Ren HL and Jin FF, 2011; Takahashi et al., 2011; Karnauskas, 2013). The EM event is characterized by a maximum sea surface temperature anomaly (SSTA) in the central equatorial Pacific,

whereas the maximum SSTA in the conventional El Niño is located in the eastern equatorial Pacific. Several studies have shown that these two types of El Niño events have different climate impacts (e.g., Weng HY et al., 2007, 2009; Feng J and Li JP, 2011; Zhang WJ et al., 2011, 2013, 2014; Xie F et al., 2012; Ren HL et al., 2016).

Ashok et al. (2007) have demonstrated that the two types of El Niño can be identified by empirical orthogonal function (EOF) analysis. For the period from 1979 to 2005, they found that the first EOF mode of the tropical Pacific represents the conventional ENSO and that the second EOF mode represents the EM (Ashok et al., 2007; Marathe et al., 2015). In addition, Trenberth and Stepaniak (2001) pointed out that the two leading modes over the tropical Pacific are closely related to ENSO and its evolution. Note that the sea surface temperature (SST) used in their study covers the period from 1979 to 1998 (Trenberth et al., 2002a). Furthermore, the leading two dominant modes associated with the ENSO and its evolution modes have been detected in the surface air temperature (e.g., Kelly and Jones, 1996) and the tropospheric and stratospheric air temperature (e.g., Yulaeva and Wallace, 1994; Fernández et al., 2004). These results suggest that the first EOF mode over the tropical Pacific represents the conventional ENSO,

Correspondence to: Q. L. Chen, chenql@cuit.edu.cn

Received 31 DEC 2018; Accepted 21 FEB 2019.

Accepted article online 25 MAR 2019.

©2019 by Earth and Planetary Physics.

which is a well-documented result (e.g., Trenberth and Stepaniak, 2001; Ashok et al., 2007; Zhang WJ et al., 2010; Li Y et al., 2015, 2017). However, the second mode of this tropical Pacific SSTA is sensitive to the study period (Feng J and Li JP, 2011).

The potential cause of the sensitive second mode is associated with the influence of global warming on the EM (Ashok et al., 2007; Yeh et al., 2009; Collins et al., 2010; Capotondi et al., 2015; Li Y et al., 2017; Lemmon and Karnauskas, 2018). Yeh et al. (2009) found that EM events did not generally occur before 1990 and that they were primarily observed during the post-1990 period. In particular, in the post-2000 period, the strongest EM event occurred between 2009 and 2010 (Lee and McPhaden, 2010). Meanwhile, Trenberth and Fasullo (2013) pointed out that the 2000s were by far the warmest decade on record, and that before then the 1990s were the warmest decade on record (their Figure 1). This suggests that more frequent EM occurrence may be closely associated with global warming. On the basis of this hypothesis, numerous studies have reported that global warming could induce more frequent EM events by modifying the background state of the tropical Pacific (Ashok et al., 2007; Yeh et al., 2009; Collins et al., 2010; Capotondi et al., 2015; Li Y et al., 2017; Lemmon and Karnauskas, 2018). These results indicate that global warming could modify the distribution of EM events during different time periods and thus affect the physical meaning of the second mode of the tropical Pacific. Because the study periods of Trenberth et al. (2002a) and Ashok et al. (2007) are different, their analyses of the second mode of the tropical Pacific are different.

These studies also raise interesting questions: What is the second dominant mode of the tropical Pacific without the global warming signal? Is it an EM mode or an evolution of ENSO? And, if the second mode is the evolution of ENSO, what is the linkage between ENSO and its evolution mode? To address these issues, the global warming signal should need to be removed. Although it is impossible at present to completely remove the global warming signal from observations, climate models provide a useful tool for analyzing climate variability without global warming. In this study, we use a long-term preindustrial control simulation from the core version of the Norwegian Climate Center's Earth System Model (NorESM1-M). We note that there is no global warming forcing in the preindustrial scenario (Taylor et al., 2012). In addition, NorESM1-M is a fully coupled model of the earth's physical climate system. A general description of the model is given in Bentsen et al. (2013) and Iversen et al. (2013).

NorESM1-M is chosen in our study because this model performs reasonably well in capturing ENSO variability. For instance, Bellenger et al. (2014) demonstrated that the modeled ENSO seasonal phase locking in NorESM1-M is very close to observations. They also showed that this model captures the spatial and temporal characteristics and Bjerknes feedback of ENSO compared with the other Phase 5 of the Coupled Model Intercomparison Project (CMIP5) models (Bellenger et al., 2014). Furthermore, numerous studies (e.g., Kim and Jin FF, 2011; Jha et al., 2014; Kim et al., 2014a, 2014b; Risbey et al., 2014; Pausata et al., 2015) have shown that NorESM1-M exhibits a more realistic portrayal of key ENSO features compared with most climate models. Considering the simulation ability of NorESM1-M in reproducing ENSO, we selec-

ted it to study the leading two modes of the tropical Pacific and their linkage without global warming.

The remainder of this article is arranged as follows. The data and methods used are described in Section 2. Section 3 investigates the leading two modes of the tropical Pacific without the influence of global warming. The potential mechanism associated with the linkage between these two leading modes is presented in Section 4. Finally, the discussion and conclusions are provided in Section 5.

2. Data and Methods

2.1 Data

The data used in this study are from the coupled atmosphere-ocean-aerosol model NorESM1-M (Bentsen et al., 2013; Iversen et al., 2013). The ocean model of NorESM1-M has a horizontal resolution of 384 (meridional grid point) \times 320 (zonal grid point) and 70 vertical levels. NorESM1-M is an Earth System Model that uses the Oslo version of the Community Atmosphere Model (i.e., CAM4-Oslo), for the atmospheric component of the model, with an updated module that simulates cycling of sea salt, mineral dust, particulate sulfate, black carbon, and primary and secondary organics. CAM4-Oslo is coupled to an updated version of the isopycnal ocean model MICOM (Miami Isopycnic Coordinate Ocean Model; Bleck and Smith, 1990; Bleck et al., 1992).

In this study, we used the preindustrial control simulation of NorESM1-M. The control simulation was integrated over 500 model years, and the last 100 years were used in the present analysis. This choice was made to avoid the initial adjustment period because of the model spin-up process. Furthermore, the 100-year segment is very similar to the period covered by common long-record observational and reanalysis data sets, such as the Hadley Centre Global Sea Ice and SST data set (Rayner et al., 2003) and the Simple Ocean Data Assimilation product (Carton and Giese, 2008). The NorESM1-M simulation data used in our analysis included variables at the sea surface (i.e., SST and surface winds) and variables in the subsurface ocean (i.e., subsurface oceanic temperature). Seasons in this article refer to the boreal season.

2.2 Methods

In this study, we used the normalized EOF, in which the principal components were divided by their standard deviation and the spatial EOF patterns were multiplied by the corresponding standard deviation (Zheng F et al., 2013). In addition, we used a lead-lag correlation. The statistical significance of the correlation between two autocorrelated time series was calculated by using the two-tailed Student's *t*-test and the effective number (N^{eff}) of degrees of freedom (Bretherton et al., 1999). For this study, N^{eff} was determined by the following approximation (e.g., Li JP et al., 2013; Xie F et al., 2016, 2017):

$$\frac{1}{N^{\text{eff}}} \approx \frac{1}{N} + \frac{2}{N} \sum_{j=1}^N \frac{N-j}{N} \rho_{XX}(j) \rho_{YY}(j), \quad (1)$$

where N is the sample size, and ρ_{XX} and ρ_{YY} are the autocorrelations of the two sampled time series, X and Y , respectively, at time

lag j .

3. Two Leading EOF Modes of the Tropical Pacific Without Global Warming

Following previous studies (Yulaeva and Wallace, 1994; Kelly and Jones, 1996; Trenberth and Stepaniak, 2001; Fernández et al., 2004; Ashok et al., 2007), we first performed an EOF analysis of SSTA in the tropical Pacific by using the preindustrial control simulation. Figure 1 shows the first two leading EOF modes over the tropical Pacific. The first two leading modes account for 43.5% and 8.0% of the total variance, respectively (Figure 1). These two modes are well separated from each other according to the criterion of North et al. (1982). The EOF1 mode depicts a typical ENSO horseshoe spatial pattern (Rasmusson and Carpenter, 1982), with the maximum SSTA in the eastern equatorial Pacific (Figure 1), whereas its normalized principal component (NPC1) is dominated by interannual variability. The power spectrum of NPC1 exhibits

dominant power around 2–7 years (not shown), which is consistent with that of ENSO. Meanwhile, Figure 2a shows the seasonal variation in the standard deviations of the NPC1. The NPC1 clearly attains the maximum variance from autumn (September–November; SON) to winter (December–February; DJF; Figure 2a), which is same as the seasonal variation of ENSO (Kug et al., 2009). In addition, strong correlation coefficients (about 0.98) were found between the NPC1 and Niño 3 and Niño 3.4 indices. These results suggest that the EOF1 mode over the tropical Pacific represents ENSO well, which is consistent with previous studies (Trenberth and Stepaniak, 2001; Trenberth et al., 2002b; Ashok et al., 2007; Zhang WJ et al., 2010; Li Y et al., 2015, 2017).

The EOF2 mode also depicts a horseshoe spatial pattern, but with cooling SSTA in the eastern equatorial Pacific (Figure 1) compared with the EOF1 or ENSO mode. Its NPC2 also exhibits interannual variability, as revealed by spectrum analysis (not shown). For the seasonal variation, the EOF2 mode has greater variance in June–August (JJA; Figure 2b). By comparing the spatial patterns

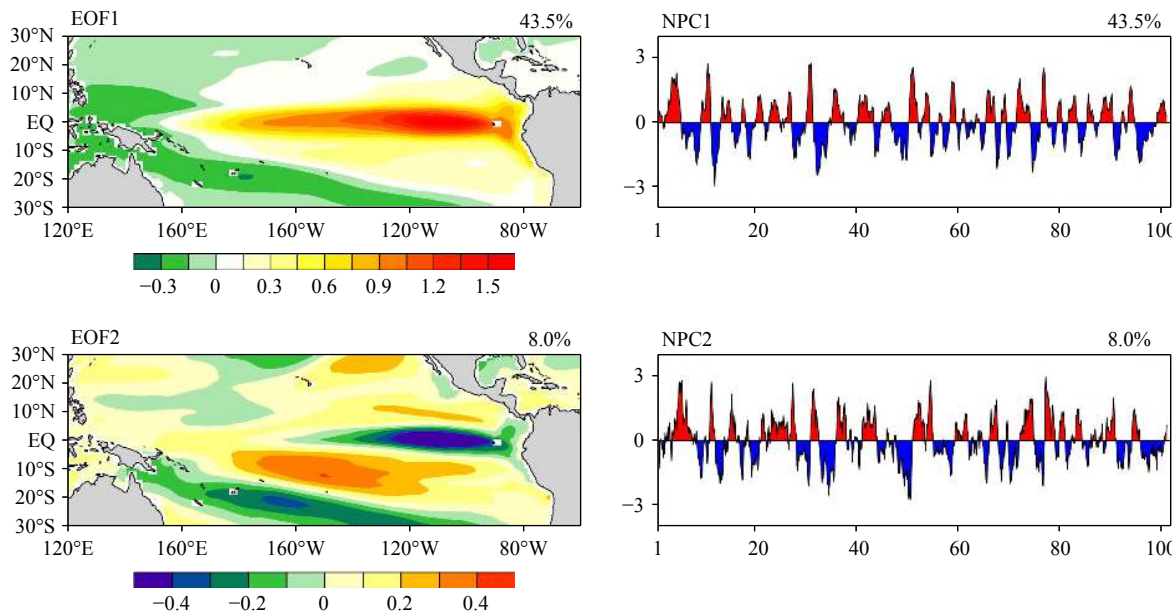


Figure 1. Spatial patterns (left) and corresponding NPCs (right) of the first two leading EOF modes of the tropical Pacific SST anomalies ($^{\circ}\text{C}$). The values of abscissa and ordinate in right panels represent the year and values of normalized principal component, respectively.

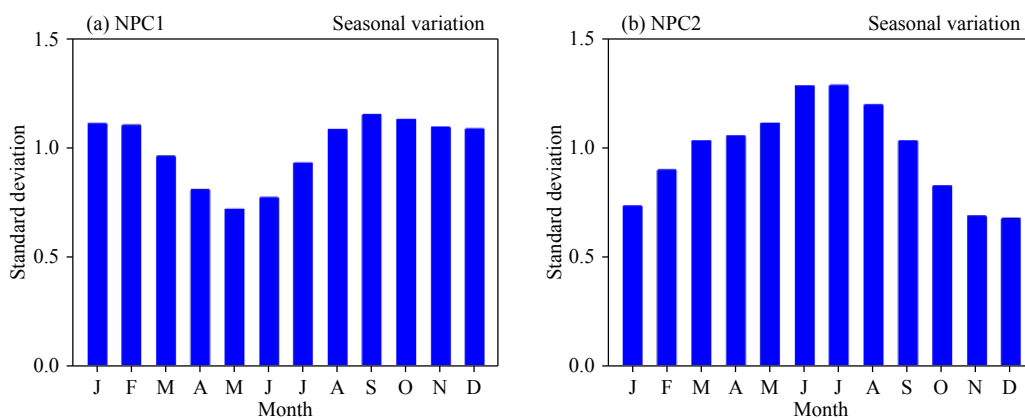


Figure 2. Seasonal variations of the standard deviation in (a) NPC1 and (b) NPC2.

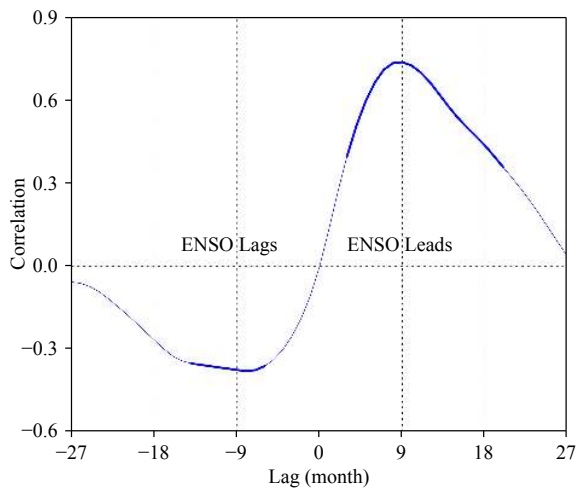


Figure 3. Lead-lag correlation between the NPCs of the ENSO and EOF2 modes. Thicker lines indicate significance at the 99% confidence level.

and peak season of the EOF2 mode and EM, it is clear that the EOF2 mode is different from the EM. In addition, the spatial pattern of EOF2 (Figure 1) is consistent with that of observational ENSO evolution in summer (JJA), as shown in Fig. 6 of Deser et al. (2010). Thus, a question to be addressed is: Does the EOF2 mode represent an aspect of the evolution of ENSO? To address this question, we calculate the lead-lag correlations between the EN-

SO mode (NPC1) and EOF2 mode (NPC2). As shown in Figure 3, the positive and negative ENSO modes lead the EOF2 mode by about 6–9 months. Note that the result of Figure 3 is consistent with that of lead-lag correlations between Niño 3 and NPC2. This lead-lag correlation supports the oscillatory sequence of the ENSO and EOF2 modes as follows: ...El Niño → EOF2 → La Niña → −EOF2 → El Niño....

Because the ENSO (EOF2) mode peaks in winter (summer; Figure 2), the SSTA pattern in the subsequent 6 months is expected to be associated with the EOF2 (negative ENSO) mode. The lead-lag correlations between the DJF-averaged NPC1 and the following year JJA-averaged SSTA are shown in Figure 4a. Hereafter, we denote the year in which the ENSO (EOF2) mode peaks in DJF (JJA) as year 0 and the preceding and following years as years −1 and +1, respectively. Figure 4a shows that the spatial pattern of the following JJA(+1) SSTA associated with the DJF(0) NPC1 depicts a horseshoe spatial pattern, with the cooling SSTA in the eastern equatorial Pacific. Note that this spatial pattern is consistent with that of lead-lag correlations between the DJF(0)-averaged Niño 3 and JJA(+1) SSTA. The pattern of Figure 4a is similar to that of the EOF2 mode (Figure 1), which is supported by their high spatial correlation coefficient (0.7). Similarly, the spatial pattern of the following DJF(0) SSTA associated with the JJA(0) NPC2 is similar to the La Niña (negative ENSO) condition. These two correlation maps agree with the oscillatory sequence of the ENSO and EOF2 modes. In summary, to a large extent, these results imply that the EOF2 mode may play an important role in the ENSO cycle, or that

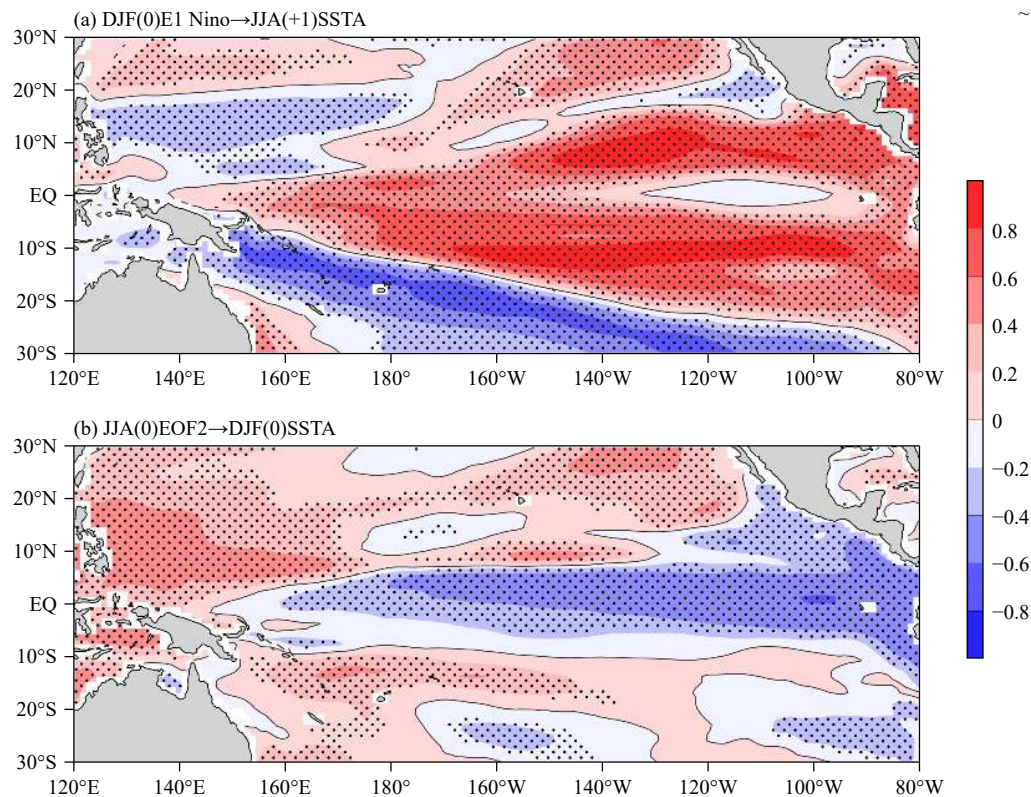


Figure 4. (a) Correlation map of the DJF(0)-averaged NPC1 with the following JJA(+1) SSTA. (b) Correlation map of the JJA(0)-averaged NPC2 with the following DJF(0) SSTA. Positive (red) and negative (blue) SSTA, with the correlation significant at the 95% level, are stippled. The thin black line denotes the zero contour.

the EOF2 mode indicates an aspect of the evolution of ENSO in the preindustrial scenario without global warming.

4. Potential Mechanism Associated with the Linkage Between ENSO and EOF2 Modes

These results show a significant lead–lag relationship between the variability in the ENSO and EOF2 modes. If the potential mechanism associated with the linkage between these two modes could be identified, it would aid in understanding whether the EOF2 mode is the evolution of ENSO. In the following section, we examine the evolutionary features of SST, surface wind, and subsurface ocean temperature anomalies associated with the EOF2 mode, with the goal of identifying the mechanism responsible for the linkage between the ENSO and EOF2 modes.

Considering that the EOF2 mode peaks in summer and that the ENSO and EOF2 modes have an oscillatory sequence, we compute lead–lag correlations between the JJA(0)-averaged NPC2 and 3-month averaged SSTA and surface wind anomalies (Figure 5). During October–February (ONDJF)(−1), about 6–9 months before the EOF2 mode peaks, significant warm SSTA occur in the central and eastern equatorial Pacific (Figures 5a–5b). At the same time,

surface wind anomalies converge in the eastern equatorial Pacific and westerly wind anomalies appear in the western equatorial Pacific. It is interesting to note that the SSTA and wind patterns shown in Figure 5b are closely related to El Niño conditions. Subsequently, the warm SSTA gradually weaken, especially in the eastern equatorial Pacific (Figures 5c–5d). During AMJ(0), easterly wind anomalies occur in the western and central equatorial Pacific. The air–sea interaction of the tropical Pacific is well known to make a dominant contribution to ENSO evolution (Bjerknes, 1969; Jin FF, 1997a, 1997b; Karnauskas, 2013; Ren HL and Jin FF, 2013; Zheng F et al., 2014, 2016). Easterly wind anomalies in the western and central equatorial Pacific lift thermocline and further induce the cooling subsurface temperature in the eastern equatorial Pacific. The accompanying strong mean upwelling in the eastern equatorial Pacific could bring up cooler subsurface waters to the near-surface layer, which in turn would cool the SST. As the easterly winds are strengthened (Figure 5d), the SSTA in the eastern equatorial Pacific becomes significantly cooler during JJA(0) (Figure 5e). Note that the SSTA pattern during JJA(0) (Figure 5e) is consistent with that of the EOF2 mode. On the basis of the air–sea interaction in the tropical Pacific, this cooler SSTA could increase the easterly wind anomalies and thus further cool the SSTA in the eastern equatorial Pacific (Figures 5f–5g). During DJF(0) and

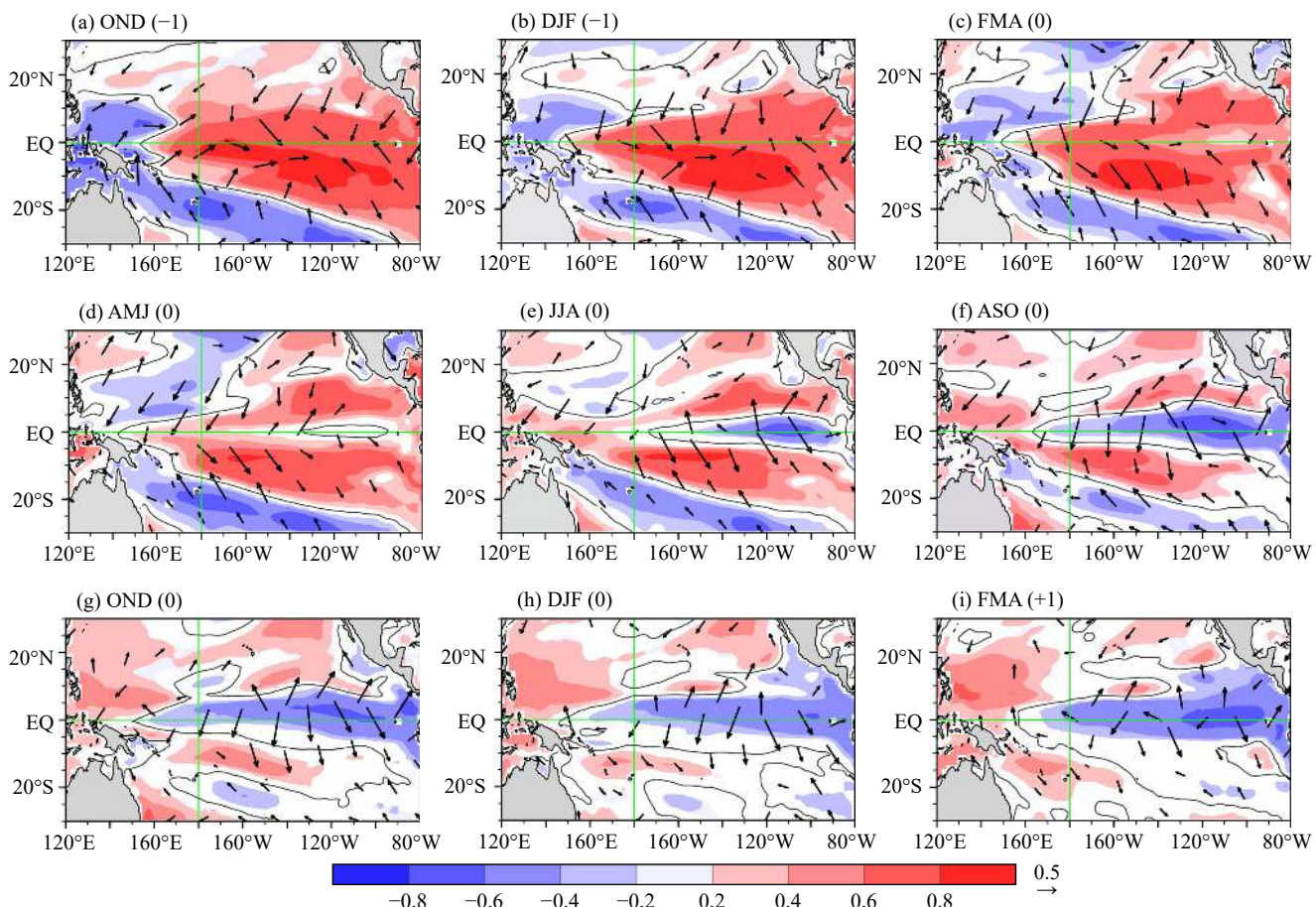


Figure 5. Correlation maps of the JJA(0)-averaged NPC2 with the 3-month averaged SSTA (shaded) and surface wind (vectors) anomalies for OND(−1), DJF(−1), FMA(0), AMJ(0), JJA(0), ASO(0), OND(0), DJF(0), and FMA(+1). Positive (red) and negative (blue) SSTA, with the correlation significant at the 95% level, are shaded. Only surface wind vectors significant at the 95% level are shown. The thin black line denotes the zero contour.

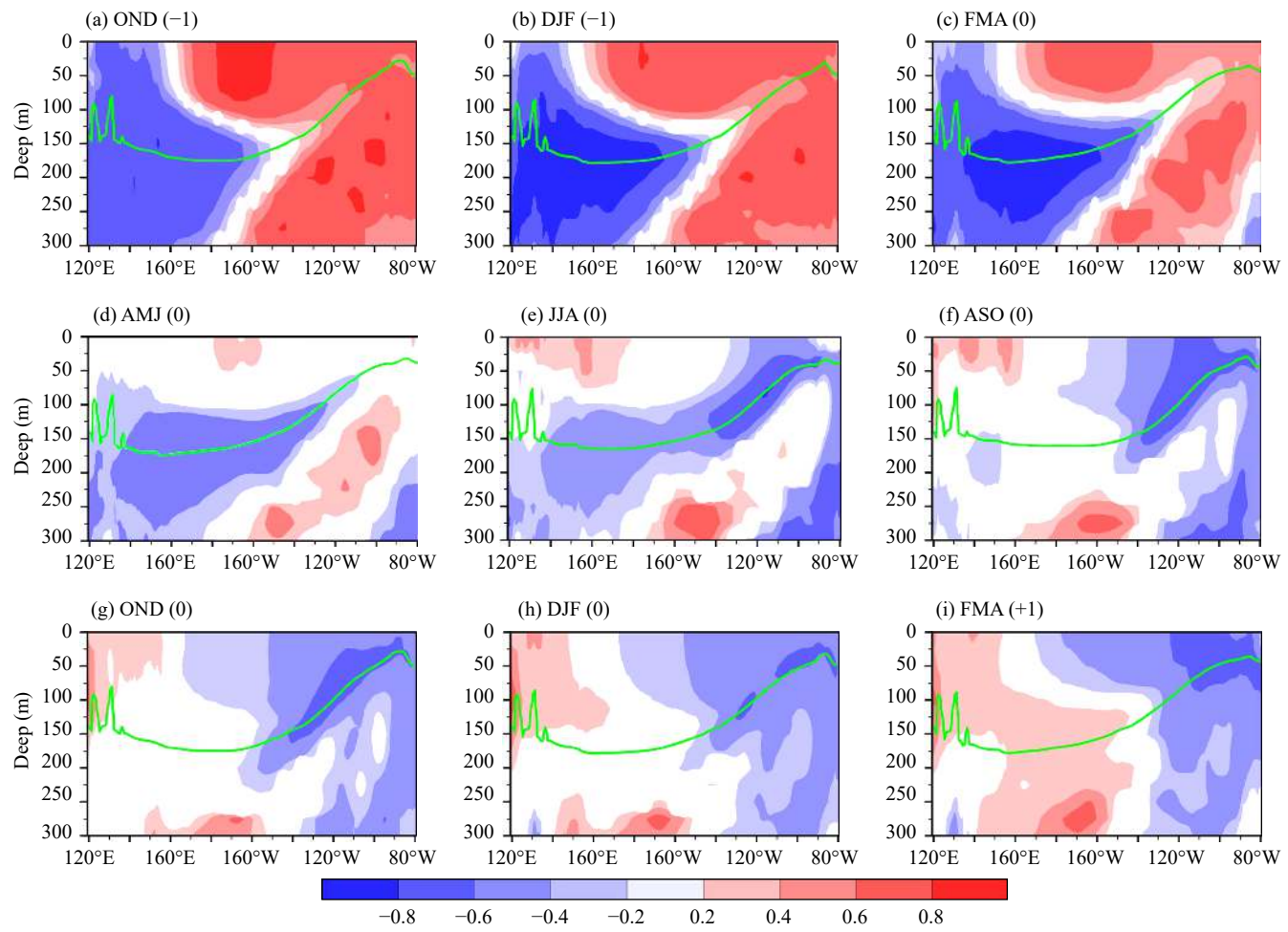


Figure 6. As in Figure 5, but for the subsurface temperature anomalies in the equatorial Pacific (5°S – 5°N). The green lines indicate the climate mean of the thermocline depth in OND, DJF, FMA, AMJ, JJA, and ASO, respectively.

FMA(+1), a horseshoe spatial pattern of cooling SSTA occurs, which is closely associated with La Niña conditions (Figures 5h–5i). These results show that the transformation between the ENSO and EOF2 modes is associated with the ENSO cycle and that the EOF2 mode is consistent with the JJA(0) SSTA pattern during ENSO evolution (Figure 5e). It is suggested that the EOF2 mode represents an aspect of the evolution of ENSO, which is similar to the results of Trenberth and Stepaniak (2001).

To illustrate the relationship between the ENSO and EOF2 modes more clearly, Figure 6 shows correlation maps of the JJA(0)-averaged NPC2 with the 3-month averaged subsurface ocean temperature anomalies at different depths averaged over 5°S – 5°N for a range of lead–lag times. During OND(JF)(−1), significant subsurface temperature anomalies in the equatorial Pacific depict a typical El Niño condition (Figures 6a–6b), which corresponds to the SSTA and surface wind anomalies shown in Figures 5a–5b. Afterward, the cooling subsurface temperature anomalies propagate eastward and upward along the thermocline (Figures 6c–6d), reaching the eastern equatorial Pacific during AMJ(0) (Figure 6d). Following previous studies (Kang et al., 2001; Jin FF et al., 2003), vigorous upwelling in the eastern equatorial Pacific could bring up cold subsurface temperature anomalies and thus cool the surface waters (Figures 5e and 6e). Once the cooling ocean temperature

anomalies are generated in the eastern equatorial Pacific (Figures 5e and 6e), easterly wind anomalies increase and the cooling of ocean temperature anomalies is further strengthened (Figures 5e–5i and 6e–6i). Finally, the subsurface temperature anomalies associated with the EOF2 mode become a La Niña condition during DJF(0) and FMA(+1). As mentioned, these results further suggest that the EOF2 mode represents an aspect of the evolution of ENSO and that the mechanism linking the ENSO and EOF2 modes is the air–sea interaction associated with ENSO cycle.

5. Discussion and Conclusions

This study investigates the first two leading EOF modes of the tropical Pacific under the preindustrial scenario. The EOF1 mode, resembling the spatial pattern of the conventional ENSO (Figure 1), attains maximum variance during autumn and winter (Figure 2a). This result suggests that the EOF1 mode over the tropical Pacific represents ENSO well, which is consistent with previous studies (Trenberth and Stepaniak, 2001; Trenberth et al., 2002b; Ashok et al., 2007; Zhang WJ et al., 2010; Li Y et al., 2015, 2017). Although the EOF2 mode also depicts a typical ENSO horseshoe spatial pattern, the cooling SSTA occurs in the eastern equatorial Pacific (Figure 1). Note that the spatial pattern of the EOF2 mode is different from that of the EM (Ashok et al., 2007). Additionally, the NPC2 at-

tains maximum variance in the summer (Figure 2b).

The significant lead–lag correlation between the ENSO and EOF2 modes (Figure 3) implies that the EOF2 mode makes an important contribution to ENSO evolution. We speculate, based on this correlation, that the ENSO and EOF2 modes occur in an oscillatory sequence as follows: ...El Niño → EOF2 → La Niña → –EOF2 → El Niño.... By studying the evolution of SST, surface wind, and subsurface ocean temperature anomalies, we find that the air–sea interaction associated with the ENSO cycle is responsible for the mechanism linking the ENSO and EOF2 modes. The present analysis suggests that the EOF2 mode represents an aspect of the evolution of ENSO and not the EM under the preindustrial scenario without global warming, which is similar to the results of Trenberth and Stepaniak (2001).

We note that our results generally agree with the conclusions of Ashok et al. (2007), who showed that the EOF2 mode represents the EM. Ashok et al. (2007) emphasized that the more frequent occurrence of EM is closely associated with global warming (Yeh et al., 2009; Collins et al., 2010; Capotondi, 2013; Li Y et al., 2017; Lemmon and Karnauskas, 2018), and our results appear to verify their conclusion from the perspective of no global warming signal. In addition, this study briefly used the NorESM1-M, which could realistically reproduce the variability and features of ENSO, to study the first two leading modes of the tropical Pacific and their linkage without global warming. In future work, we intend to use the multi-model CMIP5 to conduct further research into the two dominant modes over the tropical Pacific and their associated linkage.

Acknowledgments

This research was jointly supported by the National Key Research and Development Program on Monitoring, Early Warning and Prevention of Major Natural Disasters (2018YFC1506006), the National Natural Science Foundation of China Project (41805054, 41875108, 41805041, 41705065) and the Scientific Research Fund of the Chengdu University of Information Technology (KYTZ201724, KYTZ201602, KYTZ201727).

References

- Ashok, K., Behera, S. K., Rao, S. A., Weng, H. Y., and Yamagata, T. (2007). El Niño Modoki and its possible teleconnection. *J. Geophys. Res. Oceans*, 112(C11), C11007. <https://doi.org/10.1029/2006JC003798>
- Bellenger, H., Guilyardi, E., Leloup, J., Lengaigne, M., and Vialard, J. (2014). ENSO representation in climate models: From CMIP3 to CMIP5. *Climate Dyn.*, 42(7–8), 1999–2018. <https://doi.org/10.1007/s00382-013-1783-z>
- Bentsen, M., Bethke, I., Debernard, J. B., Iversen, T., Kirkevåg, A., Seland, Ø., Drange, H., Roelandt, C., Seierstad, I. A., ... Kristjánsson, J. E. (2013). The Norwegian earth system model, NorESM1-M—Part 1: Description and basic evaluation of the physical climate. *Geosci. Model Dev.*, 6(3), 687–720. <https://doi.org/10.5194/gmd-6-687-2013>
- Bjerknes, J. (1969). Atmospheric teleconnections from the equatorial Pacific. *Mon. Weather Rev.*, 97(3), 163–172. [https://doi.org/10.1175/1520-0493\(1969\)097<163:ATFTEP>2.3.CO;2](https://doi.org/10.1175/1520-0493(1969)097<163:ATFTEP>2.3.CO;2)
- Bleck, R., and Smith, L. T. (1990). A wind-driven isopycnic coordinate model of the north and equatorial Atlantic Ocean: 1. Model development and supporting experiments. *J. Geophys. Res. Oceans*, 95(C3), 3273–3285. <https://doi.org/10.1029/JC095iC03p03273>
- Bleck, R., Rooth, C., Hu, D. M., and Smith, L. T. (1992). Salinity-driven thermocline transients in a wind- and thermohaline-forced isopycnic coordinate model of the North Atlantic. *J. Phys. Oceanogr.*, 22(12), 1486–1505. [https://doi.org/10.1175/1520-0485\(1992\)022<1486:SDTTIA>2.0.CO;2](https://doi.org/10.1175/1520-0485(1992)022<1486:SDTTIA>2.0.CO;2)
- Bretherton, C. S., Widmann, M., Dymnikov, V. P., Wallace, J. M., and Bladé, I. (1999). The effective number of spatial degrees of freedom of a time-varying field. *J. Climate*, 12(7), 1990–2009. [https://doi.org/10.1175/1520-0442\(1999\)012<1990:TENOSD>2.0.CO;2](https://doi.org/10.1175/1520-0442(1999)012<1990:TENOSD>2.0.CO;2)
- Capotondi, A. (2013). ENSO diversity in the NCAR CCSM4 climate model. *J. Geophys. Res. Oceans*, 118(10), 4755–4770. <https://doi.org/10.1002/jgrc.20335>
- Capotondi, A., Wittenberg, A. T., Newman, M., Di Lorenzo, E., Yu, J. Y., Braconnot, P., Cole, J., Dewitte, B., Giese, B., ... Yeh, S. W. (2015). Understanding ENSO diversity. *Bull. Amer. Meteor. Soc.*, 96(6), 921–938. <https://doi.org/10.1175/BAMS-D-13-00117.1>
- Carton, J. A., and Giese, B. S. (2008). A reanalysis of ocean climate using Simple Ocean Data Assimilation (SODA). *Mon. Weather Rev.*, 136(8), 2999–3017. <https://doi.org/10.1175/2007MWR1978.1>
- Collins, M., An, S. I., Cai, W. J., Ganachaud, A., Guilyardi, E., Jin, F. F., Jochum, M., Lengaigne, M., Power, S., Timmermann, A., Vecchi, G., and Wittenberg, A. (2010). The impact of global warming on the tropical Pacific ocean and El Niño. *Nat. Geosci.*, 3(6), 391–397. <https://doi.org/10.1038/ngeo868>
- Deser, C., Alexander, M. A., Xie, S. P., and Phillips, A. S. (2010). Sea surface temperature variability: Patterns and mechanisms. *Annu. Rev. Mar. Sci.*, 2, 115–143. <https://doi.org/10.1146/annurev-marine-120408-151453>
- Feng, J., and Li, J. P. (2011). Influence of El Niño Modoki on spring rainfall over south China. *J. Geophys. Res. Atmos.*, 116(D13), D13102. <https://doi.org/10.1029/2010JD015160>
- Fernández, N. C., Herrera, R. G., Puyol, D. G., Martín, E. H., García, R. R., Presa, L. G., and Rodríguez, P. R. (2004). Analysis of the ENSO signal in tropospheric and stratospheric temperatures observed by MSU, 1979–2000. *J. Climate*, 17(20), 3934–3946. [https://doi.org/10.1175/1520-0442\(2004\)017<3934:AOTESI>2.0.CO;2](https://doi.org/10.1175/1520-0442(2004)017<3934:AOTESI>2.0.CO;2)
- Iversen, T., Bentsen, M., Bethke, I., Debernard, J. B., Kirkevåg, A., Seland, Ø., Drange, H., Kristjánsson, J. E., Medhaug, I., ... Seierstad, I. A. (2013). The Norwegian earth system model, NorESM1-M—Part 2: Climate response and scenario projections. *Geosci. Model Dev.*, 6(2), 389–415. <https://doi.org/10.5194/gmd-6-389-2013>
- Jha, B., Hu, Z. Z., and Kumar, A. (2014). SST and ENSO variability and change simulated in historical experiments of CMIP5 models. *Climate Dyn.*, 42(7–8), 2113–2124. <https://doi.org/10.1007/s00382-013-1803-z>
- Jin, F. F. (1997a). An equatorial ocean recharge paradigm for ENSO. Part I: Conceptual model. *J. Atmos. Sci.*, 54(7), 811–829. [https://doi.org/10.1175/1520-0469\(1997\)054<0811:AEORPF>2.0.CO;2](https://doi.org/10.1175/1520-0469(1997)054<0811:AEORPF>2.0.CO;2)
- Jin, F. F. (1997b). An equatorial ocean recharge paradigm for ENSO. Part II: A stripped-down coupled model. *J. Atmos. Sci.*, 54(7), 830–847. [https://doi.org/10.1175/1520-0469\(1997\)054<0830:AEORPF>2.0.CO;2](https://doi.org/10.1175/1520-0469(1997)054<0830:AEORPF>2.0.CO;2)
- Jin, F. F., An, S. I., Timmermann, A., and Zhao, J. X. (2003). Strong El Niño events and nonlinear dynamical heating. *Geophys. Res. Lett.*, 30(3), 1120. <https://doi.org/10.1029/2002GL016356>
- Kang, I. S., An, S. I., and Jin, F. F. (2001). A systematic approximation of the SST anomaly equation for ENSO. *J. Meteor. Soc. Japan*, 79(1), 1–10. <https://doi.org/10.2151/jmsj.79.1>
- Kao, H. Y., and Yu, J. Y. (2009). Contrasting eastern-Pacific and central-Pacific types of ENSO. *J. Climate*, 22(3), 615–632. <https://doi.org/10.1175/2008JCLI2309.1>
- Karnauskas, K. B. (2013). Can we distinguish canonical El Niño from Modoki?. *Geophys. Res. Lett.*, 40(19), 5246–5251. <https://doi.org/10.1002/grl.51007>
- Kelly, P. M., and Jones, P. D. (1996). Removal of the El Niño–Southern Oscillation signal from the gridded surface air temperature data set. *J. Geophys. Res. Atmos.*, 101(D14), 19013–19022. <https://doi.org/10.1029/96JD01173>
- Kim, S. T., and Jin, F. F. (2011). An ENSO stability analysis. Part II : Results from the twentieth and twenty-first century simulations of the CMIP3 models. *Climate Dyn.*, 36(7–8), 1609–1627. <https://doi.org/10.1007/s00382-010-0872-5>
- Kim, S. T., Cai, W. J., Jin, F. F., and Yu, J. Y. (2014a). ENSO stability in coupled climate models and its association with mean state. *Climate Dyn.*, 42(11–12),

- 3313–3321. <https://doi.org/10.1007/s00382-013-1833-6>
- Kim, S. T., Cai, W. J., Jin, F. F., Santoso, A., Wu, L. X., Guilyardi, E., and An, S. I. (2014b). Response of El Niño sea surface temperature variability to greenhouse warming. *Nat. Climate Change*, 4(9), 786–790. <https://doi.org/10.1038/nclimate2326>
- Kug, J. S., Jin, F. F., and An, S. I. (2009). Two types of El Niño events: Cold tongue El Niño and warm pool El Niño. *J. Climate*, 22(6), 1499–1515. <https://doi.org/10.1175/2008JCLI2642.1>
- Larkin, N. K., and Harrison, D. E. (2005). On the definition of El Niño and associated seasonal average U.S. weather anomalies. *Geophys. Res. Lett.*, 32(13), L13705. <https://doi.org/10.1029/2005GL022738>
- Lee, T., and McPhaden, M. J. (2010). Increasing intensity of El Niño in the central equatorial Pacific. *Geophys. Res. Lett.*, 37(14), L14603. <https://doi.org/10.1029/2010gl044007>
- Lemmon, D. E., and Karinauskas, K. B. (2018). A metric for quantifying El Niño pattern diversity with implications for ENSO-mean state interaction. *Climate Dyn.*, <https://doi.org/10.1007/s00382-018-4194-3>
- Li, J. P., Feng, J., and Li, Y. (2012). A possible cause of decreasing summer rainfall in northeast Australia. *Int. J. Climatol.*, 32(7), 995–1005. <https://doi.org/10.1002/joc.2328>
- Li, J. P., Sun, C., and Jin, F. F. (2013). NAO implicated as a predictor of Northern Hemisphere mean temperature multidecadal variability. *Geophys. Res. Lett.*, 40(20), 5497–5502. <https://doi.org/10.1002/2013GL057877>
- Li, Y., Li, J. P., Zhang, W. J., Zhao, X., Xie, F., and Zheng, F. (2015). Ocean dynamical processes associated with the tropical Pacific cold tongue mode. *J. Geophys. Res. Oceans*, 120(9), 6419–6435. <https://doi.org/10.1002/2015JC010814>
- Li, Y., Li, J. P., Zhang, W. J., Chen, Q. L., Feng, J., Zheng, F., Wang, W., and Zhou, X. (2017). Impacts of the tropical Pacific cold tongue mode on ENSO diversity under global warming. *J. Geophys. Res. Oceans*, 122(11), 8524–8542. <https://doi.org/10.1002/2017JC013052>
- Marathet, S., Ashok, K., Swapna, P., and Sabin, T. P. (2015). Revisiting El Niño Modoki. *Climate Dyn.*, 45(11–12), 3527–3545. <https://doi.org/10.1007/s00382-015-2555-8>
- North, G. R., Bell, T. L., Cahalan, R. F., and Moeng, F. J. (1982). Sampling errors in the estimation of empirical orthogonal functions. *Mon. Weather Rev.*, 110(7), 699–706. [https://doi.org/10.1175/1520-0493\(1982\)110<0699:SEITEO>2.0.CO;2](https://doi.org/10.1175/1520-0493(1982)110<0699:SEITEO>2.0.CO;2)
- Pausata, F. S. R., Chafik, L., Caballero, R., and Battisti, D. S. (2015). Impacts of high-latitude volcanic eruptions on ENSO and AMOC. *Proc. Natl Acad. Sci. USA*, 112(45), 13784–13788. <https://doi.org/10.1073/pnas.1509153112>
- Rasmusson, E. M., and Carpenter, T. H. (1982). Variations in tropical sea surface temperature and surface wind fields associated with the Southern Oscillation/El Niño. *Mon. Weather Rev.*, 110(5), 354–384. [https://doi.org/10.1175/1520-0493\(1982\)110<0354:VITSST>2.0.CO;2](https://doi.org/10.1175/1520-0493(1982)110<0354:VITSST>2.0.CO;2)
- Rayner, N. A., Parker, D. E., Horton, E. B., Folland, C. K., Alexander, L. V., Rowell, D. P., Kent, E. C., and Kaplan, A. (2003). Global analyses of sea surface temperature, sea ice, and night marine air temperature since the late nineteenth century. *J. Geophys. Res. Atmos.*, 108(D14), 4407. <https://doi.org/10.1029/2002JD002670>
- Ren, H. L., and Jin, F. F. (2011). Niño indices for two types of ENSO. *Geophys. Res. Lett.*, 38(4), L04704. <https://doi.org/10.1029/2010GL046031>
- Ren, H. L., and Jin, F. F. (2013). Recharge oscillator mechanisms in two types of ENSO. *J. Climate*, 26(17), 6506–6523. <https://doi.org/10.1175/JCLI-D-12-00601.1>
- Ren, H. L., Jin, F. F., Tian, B., and Scaife, A. A. (2016). Distinct persistence barriers in two types of ENSO. *Geophys. Res. Lett.*, 43(20), 10973–10979. <https://doi.org/10.1002/2016GL071015>
- Risbey, J. S., Lewandowsky, S., Langlais, C., Monselesan, D. P., O'Kane, T. J., and Oreskes, N. (2014). Well-estimated global surface warming in climate projections selected for ENSO phase. *Nat. Climate Change*, 4(9), 835–840. <https://doi.org/10.1038/nclimate2310>
- Takahashi, K., Montecinos, A., Goubanova, K., and Dewitte, B. (2011). ENSO regimes: Reinterpreting the canonical and Modoki El Niño. *Geophys. Res. Lett.*, 38(10), L10704. <https://doi.org/10.1029/2011GL047364>
- Taylor, K. E., Stouffer, R. J., and Meehl, G. A. (2012). An overview of CMIP5 and the experiment design. *Bull. Amer. Meteor. Soc.*, 93(4), 485–498. <https://doi.org/10.1175/BAMS-D-11-00094.1>
- Trenberth, K. E., and Stepaniak, D. P. (2001). Indices of El Niño evolution. *J. Climate*, 14(8), 1697–1701. [https://doi.org/10.1175/1520-0442\(2001\)014<1697:LIOENO>2.0.CO;2](https://doi.org/10.1175/1520-0442(2001)014<1697:LIOENO>2.0.CO;2)
- Trenberth, K. E., Stepaniak, D. P., and Caron, J. M. (2002a). Interannual variations in the atmospheric heat budget. *J. Geophys. Res. Atmos.*, 107(D8), AAC 4–1–AAC 4–15. <https://doi.org/10.1029/2000JD000297>
- Trenberth, K. E., Caron, J. M., Stepaniak, D. P., and Worley, S. (2002b). Evolution of El Niño-Southern Oscillation and global atmospheric surface temperatures. *J. Geophys. Res. Atmos.*, 107(D8), AAC 5–1–AAC 5–17. <https://doi.org/10.1029/2000JD000298>
- Trenberth, K. E., and Fasullo, J. T. (2013). An apparent hiatus in global warming?. *Earth's Future*, 1(1), 19–32. <https://doi.org/10.1002/2013EF000165>
- Wallace, J. M., and Gutzler, D. S. (1981). Teleconnections in the geopotential height field during the Northern Hemisphere winter. *Mon. Weather Rev.*, 109(4), 784–812. [https://doi.org/10.1175/1520-0493\(1981\)109<0784:TITGHF>2.0.CO;2](https://doi.org/10.1175/1520-0493(1981)109<0784:TITGHF>2.0.CO;2)
- Weng, H. Y., Ashok, K., Behera, S. K., Rao, S. A., and Yamagata, T. (2007). Impacts of recent El Niño Modoki on dry/wet conditions in the Pacific rim during boreal summer. *Climate Dyn.*, 29(2–3), 113–129. <https://doi.org/10.1007/s00382-007-0234-0>
- Weng, H. Y., Behera, S. K., and Yamagata, T. (2009). Anomalous winter climate conditions in the Pacific rim during recent El Niño Modoki and El Niño events. *Climate Dyn.*, 32(5), 663–674. <https://doi.org/10.1007/s00382-008-0394-6>
- Xie, F., Li, J., Tian, W., Feng, J., and Huo, Y. (2012). Signals of El Niño Modoki in the tropical tropopause layer and stratosphere. *Atmos. Chem. Phys.*, 12(11), 5259–5273. <https://doi.org/10.5194/acp-12-5259-2012>
- Xie, F., Li, J. P., Tian, W. S., Fu, Q., Jin, F. F., Hu, Y. Y., Zhang, J. K., Wang, W. K., Sun, C., ... Ding, R. Q. (2016). A connection from Arctic stratospheric ozone to El Niño-Southern oscillation. *Environ. Res. Lett.*, 11(12), 124026. <https://doi.org/10.1088/1748-9326/11/12/124026>
- Xie, F., Li, J. P., Zhang, J. K., Tian, W. S., Hu, Y. Y., Zhao, S., Sun, C., Ding, R. Q., Feng, J., and Yang, Y. (2017). Variations in North Pacific sea surface temperature caused by Arctic stratospheric ozone anomalies. *Environ. Res. Lett.*, 12(11), 114023. <https://doi.org/10.1088/1748-9326/aa9005>
- Yang, R. W., Xie, Z., and Cao, J. (2017). A dynamic index for the westward ridge point variability of the Western Pacific subtropical high during summer. *J. Climate*, 30(9), 3325–3341. <https://doi.org/10.1175/JCLI-D-16-0434.1>
- Yang, R. W., Wang, J., Zhang, T. Y., and He, S. P. (2019). Change in the relationship between the Australian summer monsoon circulation and boreal summer precipitation over Central China in the late 1990s. *Meteor. Atmos. Phys.*, 131(1), 105–113. <https://doi.org/10.1007/s00703-017-0556-3>
- Yeh, S. W., Kug, J. S., Dewitte, B., Kwon, M. H., Kirtman, B. P., and Jin, F. F. (2009). El Niño in a changing climate. *Nature*, 461(7263), 511–514. <https://doi.org/10.1038/nature08316>
- Yulaeva, E., and Wallace, J. M. (1994). The signature of ENSO in global temperature and precipitation fields derived from the microwave sounding unit. *J. Climate*, 7(11), 1719–1736. [https://doi.org/10.1175/1520-0442\(1994\)007<1719:TSOEIG>2.0.CO;2](https://doi.org/10.1175/1520-0442(1994)007<1719:TSOEIG>2.0.CO;2)
- Zhang, W. J., Li, J. P., and Zhao, X. (2010). Sea surface temperature cooling mode in the Pacific cold tongue. *J. Geophys. Res. Oceans*, 115(C12), C12042. <https://doi.org/10.1029/2010JC006501>
- Zhang, W. J., Jin, F. F., Li, J. P., and Ren, H. L. (2011). Contrasting impacts of two-type El Niño over the western north Pacific during boreal autumn. *J. Meteor. Soc. Japan*, 89(5), 563–569. <https://doi.org/10.2151/jmsj.2011-510>
- Zhang, W. J., Jin, F. F., Zhao, J. X., Qi, L., and Ren, H. L. (2013). The possible influence of a nonconventional El Niño on the severe autumn drought of 2009 in southwest China. *J. Climate*, 26(21), 8392–8405. <https://doi.org/10.1175/JCLI-D-12-00851.1>
- Zhang, W. J., Jin, F. F., and Turner, A. (2014). Increasing autumn drought over southern China associated with ENSO regime shift. *Geophys. Res. Lett.*, 41(11), 4020–4026. <https://doi.org/10.1002/2014GL060130>

- Zheng, F., Zhu, J., Zhang, R. H., and Zhou, G. Q. (2006). Ensemble hindcasts of SST anomalies in the tropical Pacific using an intermediate coupled model. *Geophys. Res. Lett.*, 33(19), L19604. <https://doi.org/10.1029/2006GL026994>
- Zheng, F., Li, J. P., Clark, R. T., and Nnamchi, H. C. (2013). Simulation and projection of the Southern Hemisphere annular mode in CMIP5 models. *J. Climate*, 26(24), 9860–9879. <https://doi.org/10.1175/JCLI-D-13-00204.1>
- Zheng, F., Fang, X. H., Yu, J. Y., and Zhu, J. (2014). Asymmetry of the Bjerknes positive feedback between the two types of El Niño. *Geophys. Res. Lett.*, 41(21), 7651–7657. <https://doi.org/10.1002/2014GL062125>
- Zheng, F., and Zhu, J. (2016). Improved ensemble-mean forecasting of ENSO events by a zero-mean stochastic error model of an intermediate coupled model. *Climate Dyn.*, 47(12), 3901–3915. <https://doi.org/10.1007/s00382-016-3048-0>
- Zheng, F., Fang, X. H., Zhu, J., Yu, J. Y., and Li, X. C. (2016). Modulation of Bjerknes feedback on the decadal variations in ENSO predictability. *Geophys. Res. Lett.*, 43(24), 12560–12568. <https://doi.org/10.1002/2016GL071636>
- Zheng, F., and Yu, J. Y. (2017). Contrasting the skills and biases of deterministic predictions for the two types of El Niño. *Adv. Atmos. Sci.*, 34(12), 1395–1403. <https://doi.org/10.1007/s00376-017-6324-y>